

## Conformations of Silica-Bound (Pentafluorophenyl)propyl Groups Determined by Solid-State NMR Spectroscopy and Theoretical Calculations

Kanmi Mao,<sup>†</sup> Takeshi Kobayashi,<sup>†</sup> Jerzy W. Wiench,<sup>†</sup> Hung-Ting Chen,<sup>†,‡</sup>  
Chih-Hsiang Tsai,<sup>‡</sup> Victor S.-Y. Lin,<sup>†,‡</sup> and Marek Pruski<sup>\*,†,‡</sup>

*U.S. DOE Ames Laboratory, and Department of Chemistry, Iowa State University,  
Ames, Iowa 50011*

Received June 8, 2010; E-mail: mpruski@iastate.edu

**Abstract:** The conformations of (pentafluorophenyl)propyl groups ( $-\text{CH}_2-\text{CH}_2-\text{CH}_2-\text{C}_6\text{F}_5$ , abbreviated as PFP), covalently bound to the surface of mesoporous silica nanoparticles (MSNs), were determined by solid-state NMR spectroscopy and further refined by theoretical modeling. Two types of PFP groups were described, including molecules in the prone position with the perfluorinated aromatic rings located above the siloxane bridges (PFP-p) and the PFP groups denoted as upright (PFP-u), whose aromatic rings do not interact with the silica surface. Two-dimensional (2D)  $^{13}\text{C}-^1\text{H}$ ,  $^{13}\text{C}-^{19}\text{F}$  and  $^{19}\text{F}-^{29}\text{Si}$  heteronuclear correlation (HETCOR) spectra were obtained with high sensitivity on natural abundance samples using fast magic angle spinning (MAS), indirect detection of low- $\gamma$  nuclei and signal enhancement by Carr–Purcell–Meiboom–Gill (CPMG) spin–echo sequence. 2D double-quantum (DQ)  $^{19}\text{F}$  MAS NMR spectra and spin–echo measurements provided additional information about the structure and mobility of the pentafluorophenyl rings. Optimization of the PFP geometry, as well as calculations of the interaction energies and  $^{19}\text{F}$  chemical shifts, proved very useful in refining the structural features of PFP-p and PFP-u functional groups on the silica surface. The prospects of using the PFP-functionalized surface to modify its properties (e.g., the interaction with solvents, especially water) and design new types of the heterogeneous catalytic system are discussed.

### Introduction

In spite of a long history of organofluorine chemistry, fluorocarbons are of growing interest in academic studies and chemical industry.<sup>1–7</sup> Due to high electronegativity and low electron polarizability of fluorine, the physical and chemical properties of these compounds differ from those of their hydrocarbon analogues. They exhibit extremely weak intermolecular van der Waals interactions, which gives rise to high volatility, low refractive index and small surface tension.<sup>8,9</sup> Accordingly, modification of surface by fluorocarbons can influence the surface wettability. Indeed, a monolayer of  $\text{CF}_3(\text{CF}_2)_{10}\text{CO}_2\text{H}$  molecules on platinum produced a nonwetable

surface with the lowest tension value (6 dyn/cm) ever reported.<sup>10</sup> Similarly, an “ultrahydrophobic” surface was formed on the silicon wafer via layer-by-layer sequential adsorption of perfluorinated polyelectrolytes.<sup>11</sup> Several mesoporous silica materials with fluorocarbon-modified surfaces have been recently reported.<sup>12–14</sup> For example, Corma and colleagues synthesized a mesoporous silica material with immobilized perfluorosulfonic acid and used it as a catalyst for esterification and acylation. The studies have shown that the surface properties of mesoporous channels can be strongly influenced by the presence of fluorocarbons, even when the surface coverage is only a fraction of a monolayer.

The goal of the present study is to demonstrate that the fundamental properties of surface-bound fluorocarbon molecules can be investigated in unprecedented detail by using the advanced two-dimensional solid-state NMR experiments and theoretical calculations. Specifically, we focus on understanding the molecular structure and conformation of the surface-bound PFP groups in the mesoporous silica nanoparticles (MSNs). The

<sup>†</sup> Ames Laboratory, Iowa State University.

<sup>‡</sup> Department of Chemistry, Iowa State University.

- (1) Curran, D. P. *Angew. Chem., Int. Ed.* **1998**, *37*, 1175–1196.
- (2) Zhang, W.; Curran, D. P. *Tetrahedron* **2006**, *62*, 11837–11865.
- (3) Dolbier, W. R., Jr. *J. Fluorine Chem* **2005**, *126*, 157–163.
- (4) Lemal, D. M. *J. Org. Chem.* **2004**, *69*, 1–11.
- (5) Ueyama, K.; *Organofluorine Chemistry*; Wiley-Blackwell: Oxford, U.K., 2006.
- (6) Banks, R. E.; Smart, B. E.; Tatlow, J. C., Eds.; *Organofluorine Chemistry: Principles and Commercial Applications*; Springer: New York, 1994.
- (7) Hiyama, T. *Organofluorine Compounds: Chemistry and Applications*; Springer: New York, 2000.
- (8) Persico, D. F.; Lagow, R. J.; Clark, L. C., Jr.; Huang, H.-N. *J. Org. Chem.* **1985**, *50*, 5156–5159.
- (9) Slinn, D. S. L.; Green, S. W. In *Properties and Industrial Applications of Organofluorine Compounds*; Banks, R. E., Ed.; Ellis Horwood: Chichester, 1982; pp 45–82.

- (10) Hare, E. F.; Shafrin, E. G.; Zisman, W. A. *J. Phys. Chem.* **1954**, *58*, 236–239.
- (11) Jisr, R. M.; Rmaile, H. H.; Schlenoff, J. B. *Angew. Chem., Int. Ed.* **2005**, *44*, 782–785.
- (12) Kumar, R.; Chen, H.-T.; Escoto, J. L. V.; Lin, V. S. Y.; Pruski, M. *Chem. Mater.* **2006**, *18*, 4319–4327.
- (13) Alvaro, M.; Corma, A.; Das, D.; Fornes, V.; Garcia, H. *J. Catal.* **2005**, *231*, 48–55.
- (14) Alvaro, M.; Corma, A.; Das, D.; Fornes, V.; Garcia, H. *Chem. Commun.* **2004**, 956–957.

NMR studies used newly developed schemes for enhancement of sensitivity under fast magic angle spinning (MAS), which enabled the detection of heteronuclear correlation (HETCOR) spectra of naturally abundant  $^{13}\text{C}$  and  $^{29}\text{Si}$  nuclei on the silica surface with exceptional sensitivity. The theoretical investigations provided invaluable assistance in refining the conformational details of two types of PFP species described by NMR.

## Materials and Methods

**PFP-MSN Material.** The sample containing (pentafluorophenyl)propyl groups ( $-\text{CH}_2-\text{CH}_2-\text{CH}_2-\text{C}_6\text{F}_5$ ) covalently bound to MSNs, referred to as PFP-MSN, was synthesized via the previously reported cocondensation method.<sup>12,15–18</sup> A mixture of cetyltrimethylammonium bromide (1.0 g, 2.75 mmol), 2 M NaOH(aq) (3.5 mL, 7.0 mmol), and 480 mL of  $\text{H}_2\text{O}$  was stirred at 80 °C for 10 min, followed by the addition of tetraethoxysilane (TEOS, 5 mL, 22.4 mmol) and [(pentafluorophenyl)propyl]trimethoxysilane (0.58 mL, 2.24 mmol). The solution was maintained at 80 °C for 2 h and separated by filtration. The resulting product was sequentially washed with water, methanol, and dried under vacuum yielding 1.0 g of as-made PFP-MSN. The surfactant was removed using acid extraction, by refluxing the as-made PFP-MSN in methanolic solution of hydrochloric acid (1.0 mL of concentrated HCl in 100 mL of MeOH) for 6 h. After filtration and extensive washing with water and methanol, 0.7 g of the surfactant-free PFP-MSN was obtained in the form of white fine powder.<sup>12</sup>

The TEM micrograph of PFP-MSN (not shown) indicated that the particles had elliptical shape with an average length of 300 nm and an aspect ratio of 1.5–2. The parallel, cylindrical pores formed a hexagonal mesostructure, as further confirmed by powder XRD experiments. The measured BET surface area and the pore diameter were  $844 \pm 10 \text{ m}^2/\text{g}$  and  $2.2 \pm 0.2 \text{ nm}$ , respectively. Based on the analysis of nitrogen adsorption, the mesopore volume was estimated at  $0.75 \text{ cm}^3/\text{g}$ .

**Solid-State NMR.** Solid-state NMR experiments were performed on a Varian NMR System spectrometer, equipped with a 1.6 mm triple resonance FastMAS probe and operated at 599.6 MHz for  $^1\text{H}$ , 564.2 MHz for  $^{19}\text{F}$ , 150.8 MHz for  $^{13}\text{C}$  and 119.1 MHz for  $^{29}\text{Si}$  nuclei. The sample was packed in the MAS rotor after the exposure to ambient conditions in the laboratory. Several one-dimensional (1D) and two-dimensional (2D) experiments were used, including 1D MAS with direct polarization (DPMAS), spin-echo, 2D through-bond and through-space HETCOR NMR utilizing the refocused INEPT (INEPTR) and cross-polarization (CP), respectively, and 2D double-quantum (DQ) MAS NMR. To increase the sensitivity, the  $^1\text{H}$ – $^{13}\text{C}$  and  $^{19}\text{F}$ – $^{13}\text{C}$  HETCOR experiments were performed with indirect detection of heteronuclei ( $^{13}\text{C}$ ) under fast MAS.<sup>19–21</sup> The pulse sequences used in the indirectly detected through-space and through-bond HETCOR experiments are analogous to those reported elsewhere.<sup>20,21</sup> The  $^{19}\text{F}$ – $^{29}\text{Si}$  HETCOR spectra were acquired using cross-polarization and the Carr–Purcell–Meiboom–Gill (CPMG) refocusing of  $^{29}\text{Si}$  magnetization.<sup>22,23</sup>

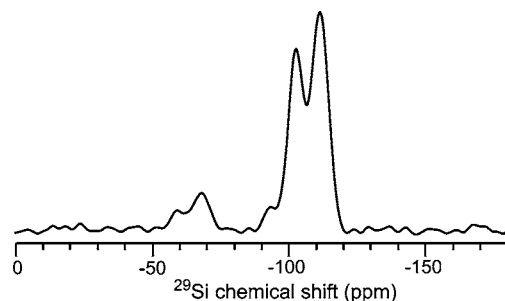


**Figure 1.**  $^{29}\text{Si}$  DPMAS NMR spectrum of PFP-MSN taken under the following experimental conditions:  $\nu_{\text{R}} = 10 \text{ kHz}$ ,  $\nu_{\text{RF}}^{\text{Si}} = 86 \text{ kHz}$  during short pulses,  $\nu_{\text{RF}}^{\text{H}} = 45 \text{ kHz}$  during TPPM decoupling,  $N_{\text{CPMG}} = 25$ ,  $\tau_{\text{CPMG}} = 6 \text{ ms}$ ,  $\tau_{\text{RD}} = 300 \text{ s}$  and  $\text{NS} = 120$ .

The experimental parameters are given in figure captions, using the following symbols:  $\nu_{\text{R}}$  denotes the magic angle spinning (MAS) rate,  $\nu_{\text{RF}}^{\text{X}}$  the magnitude of the RF magnetic field applied to X spins,  $\tau_{\text{CP}}$  the cross-polarization time,  $\tau_1$  and  $\tau_2$  the delays used during refocused INEPT,  $\tau_{\text{RR}}$  the rotary resonance recoupling time,  $N_{\text{CPMG}}$  the number of echoes used during the CPMG acquisition,  $\tau_{\text{CPMG}}$  the time interval between  $\pi$  pulses in the CPMG sequence,  $\Delta t_1$  the increment of  $t_1$  during 2D acquisition, NS the number of scans,  $\tau_{\text{RD}}$  the recycle delay, and AT the total acquisition time of a 2D spectrum. The  $^1\text{H}$ ,  $^{13}\text{C}$  and  $^{29}\text{Si}$  chemical shifts are reported using the  $\delta$  scale and are referenced to TMS at 0 ppm. The  $^{19}\text{F}$  NMR spectra are referred to  $\text{CFCl}_3$  ( $\delta = 0 \text{ ppm}$ ), based on substitution of the secondary reference of NaF aqueous solution ( $-121.5 \text{ ppm}$ ).<sup>24</sup>

**Theoretical Calculations.** The geometry of the PFP functional group inside the MSN was studied by theoretical calculations using  $\text{C}_6\text{F}_6$  and Si-containing cluster models for the surface oxygen sites of the MSN, as described in Results and Discussion. The geometries of the models were first approximated by the MM2 level calculations and further refined with the quantum mechanical theory using the Firefly program package.<sup>25,26</sup> The quantum mechanical calculations were carried out at the Møller–Plesset second-order perturbation theory (MP2) level with the 6-311++G(d,p) basis set. The interaction energies in the optimized geometries were corrected for the basis set superposition error (BSSE) using the counterpoise method.<sup>27</sup> Density functional theory (DFT) calculations of the NMR tensors were carried out at the B3LYP level using ORCA program package.<sup>28</sup> An IGLO-II type basis set<sup>29</sup> was employed in the DFT calculations. Theoretical shieldings were transformed to relative chemical shifts  $\delta$  by subtracting the calculated chemical shift of  $\text{CFCl}_3$ .

## Results and Discussion

**Solid-State NMR.** The  $^{29}\text{Si}$  DPMAS spectrum of PFP-MSN (Figure 1) is dominated by resonance lines at around  $-113$  and  $-104 \text{ ppm}$  representing silicon sites  $\text{Q}^4$  ( $(\equiv\text{SiO}-)_4\text{Si}$ ) and  $\text{Q}^3$  ( $(\equiv\text{SiO}-)_3\text{Si}(-\text{OH})$ ), respectively. The presence of peaks centered at around  $-70$  and  $-60 \text{ ppm}$ , which are assigned to silicon atoms in positions  $(\text{SiO})_3\text{SiR}$  and  $(\text{SiO})_2\text{Si}(\text{OH})\text{R}$  (de-

- (15) Chen, H.-T.; Huh, S.; Lin, V. S. Y. In *Catalyst Preparation*; Regalbuto, J., Ed.; CRC Press: Boca Raton, 2007; pp 45–74.
- (16) Chen, H. T.; Huh, S.; Wiench, J. W.; Pruski, M.; Lin, V. S. Y. *J. Am. Chem. Soc.* **2005**, *127*, 13305–13311.
- (17) Huh, S.; Chen, H. T.; Wiench, J. W.; Pruski, M.; Lin, V. S. Y. *Angew. Chem., Int. Ed.* **2005**, *44*, 1826–1830.
- (18) Huh, S.; Chen, H. T.; Wiench, J. W.; Pruski, M.; Lin, V. S. Y. *J. Am. Chem. Soc.* **2004**, *126*, 1010–1011.
- (19) Ishii, Y.; Tycko, R. *J. Magn. Reson.* **2000**, *142*, 199–204.
- (20) Wiench, J. W.; Bronnimann, C. E.; Lin, V. S. Y.; Pruski, M. *J. Am. Chem. Soc.* **2007**, *129*, 12076–12077.
- (21) Mao, K.; Wiench, J. W.; Lin, V. S. Y.; Pruski, M. *J. Magn. Reson.* **2009**, *196*, 92–95.
- (22) Wiench, J. W.; Lin, V. S. Y.; Pruski, M. *J. Magn. Reson.* **2008**, *193*, 233–242.
- (23) Trebosch, J.; Wiench, J. W.; Huh, S.; Lin, V. S. Y.; Pruski, M. *J. Am. Chem. Soc.* **2005**, *127*, 7587–7593.

- (24) Chekmenev, E. Y.; Chow, S. K.; Tofan, D.; Weitekamp, D. P.; Ross, B. D.; Bhattacharya, P. *J. Phys. Chem. B* **2008**, *112*, 6285–6287.
- (25) Granovsky, A. A. *Firefly*, version 7.1.G; <http://classic.chem.msu.su/gran/firefly/index.html>.
- (26) Schmidt, M. W.; Baldrige, K. K.; Boatz, J. A.; Elbert, S. T.; Gordon, M. S.; Jensen, J. H.; Koseki, S.; Matsunaga, N.; Nguyen, K. A.; Su, S. J.; Windus, T. L.; Dupuis, M.; Montgomery, J. A. *J. Comput. Chem.* **1993**, *14*, 1347–1363.
- (27) Boys, S. F.; Bernardi, F. *Mol. Phys.* **1970**, *19*, 553–566.
- (28) Nesse, F. *ORCA-An Ab initio, DFT and Semiempirical Electronic Structure Package*, Ver. 2.7.0; 2010.
- (29) Kutzelnigg, W.; Fleischer, U.; Schindler, M. *The IGLO-Method: Ab Initio Calculation and Interpretation of NMR Chemical Shifts and Magnetic Susceptibilities*; Springer-Verlag: Heidelberg, 1990; Vol. 23.

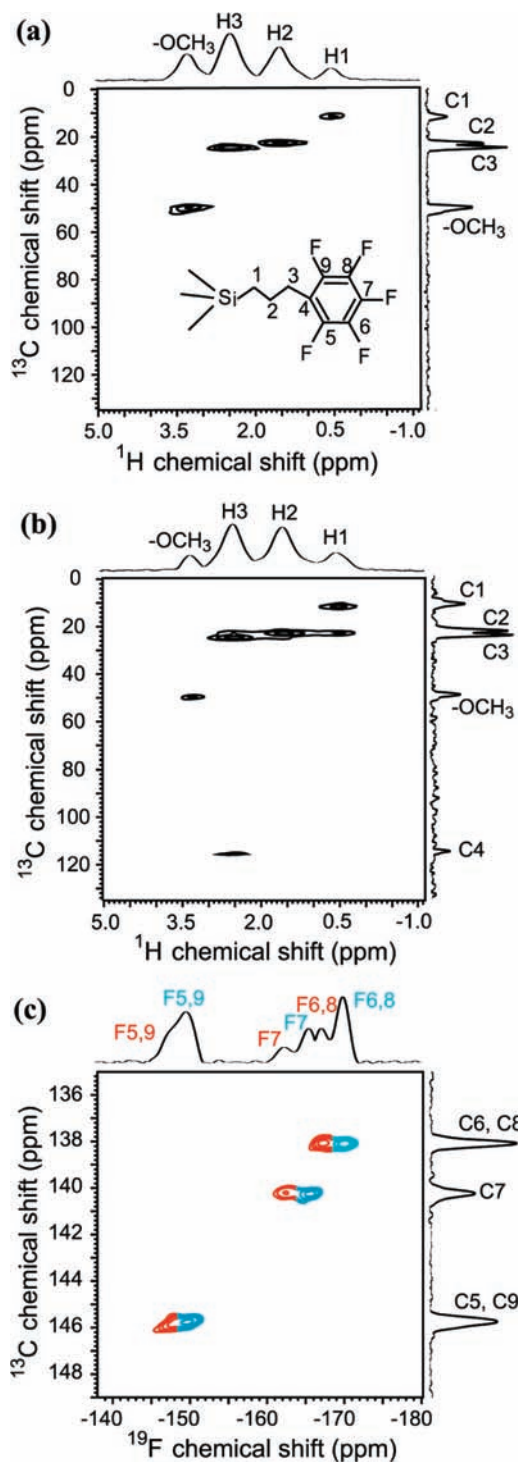


**Figure 2.** 2D indirectly detected  $^{13}\text{C}$ – $^1\text{H}$  (a, b) and  $^{13}\text{C}$ – $^{19}\text{F}$  (c) spectra of PFP-MSN. Spectra (a) and (b), obtained using through-bond (INEPT) and through-space (CP) mixing, were used in our earlier report on indirect detection.<sup>21</sup> They were recorded using  $\nu_{\text{R}} = 40$  kHz,  $\nu_{\text{RF}}^{\text{H}} = 110$  kHz during short pulses,  $\nu_{\text{RF}}^{\text{H}} = 60$  kHz during tangent ramp CP,  $\nu_{\text{RF}}^{\text{H}} = 20$  kHz during  $\tau_{\text{RR}}$ ,  $\nu_{\text{RF}}^{\text{F}} = 100$  kHz during short pulses and CP,  $\nu_{\text{RF}}^{\text{F}} = 10$  kHz during SPINAL-64 decoupling,  $\tau_{\text{CP}} = 4.5$  ms,  $\tau_1 = 0.6$  ms,  $\tau_2 = 0.8$  ms,  $\tau_{\text{RR}} = 80$  ms, 160 rows with  $\Delta t_1 = 25$   $\mu\text{s}$ , 128 (a) and 48 (b) scans per row,  $\tau_{\text{RD}} = 1.5$  s, and AT = 12.5 h (a) and 4.5 h (b). Spectrum (c) was obtained using INEPT under similar conditions, exclusive of  $\tau_1 = 1.0$  ms,  $\tau_2 = 0.9$  ms, 80 rows,  $\Delta t_1 = 200$   $\mu\text{s}$ , 400 scans per row,  $\tau_{\text{RD}} = 0.8$  s, and AT = 15.5 h.

noted as T<sup>3</sup> and T<sup>2</sup>), shows that the organic groups are indeed covalently bound to the surface.<sup>22</sup> Based on integration of the  $^{29}\text{Si}$  DPMAS spectrum we estimated that  $13 \pm 2\%$  of silicon

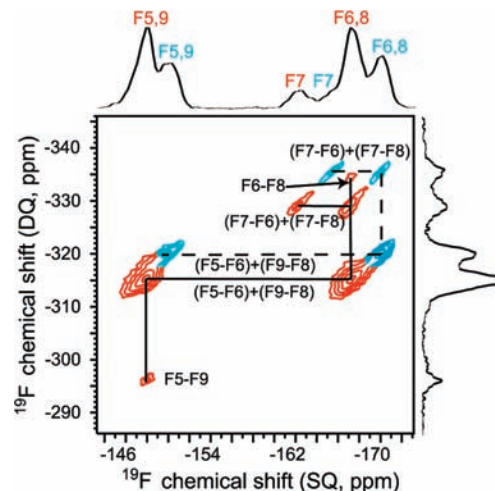


**Figure 3.** 2D  $^{19}\text{F}$ – $^{19}\text{F}$  DQMAS spectrum of PFP-MSN. The DQ excitation and reconversion was achieved using back-to-back (BABA) pulse sequence,<sup>31</sup>  $\nu_{\text{R}} = 40$  kHz,  $\nu_{\text{RF}}^{\text{F}} = 110$  kHz, and excitation/reconversion length = 0.4 ms. The spectrum was acquired in 80 rows, with 128 scans per row,  $\Delta t_1 = 25$   $\mu\text{s}$ ,  $\tau_{\text{RD}} = 1$  s, and AT = 6 h.

atoms in this sample are bound to carbon, which corresponds to the PFP concentration of 1.2 mmol/g, or roughly 1 molecule per  $\text{nm}^2$ . This last estimate was made by assuming that the inner pore surface area in PFP-MSN constitutes 90% of the total surface area of 844  $\text{m}^2/\text{g}$ . Since the footprint area of the PFP complex is  $\sim 0.6$   $\text{nm}^2$ , this concentration would correspond to surface coverage of around 60%, if all molecules assumed the prone position.

With the static  $^1\text{H}$  and  $^{19}\text{F}$  linewidths being on the order of 10–20 kHz, the 2D HETCOR spectra of PFP-MSN could be best measured using the indirect detection of heteronuclei under fast MAS.<sup>19–21</sup> The indirectly detected, INEPT-based  $^{13}\text{C}$ – $^1\text{H}$  spectrum of PFP-MSN is shown in Figure 2a. The observed correlations between directly bound C1–H1, C2–H2 and C3–H3 pairs are consistent with the expected structure of the PFP groups covalently attached to the silica surface. Also observed is a resonance due to surface methoxy functionality, as shown in our earlier report.<sup>21</sup> The same correlations, as well as those due to long-range, through-space interactions between C2–H1, C2–H3 and C3–H2 are observed in the spectrum derived through space with  $\tau_{\text{CP}} = 4.5$  ms (Figure 2b). Also observed in Figure 2b is the correlation between H3 and the aromatic ring (carbon C4).

In the  $^{13}\text{C}$ – $^{19}\text{F}$  HETCOR spectrum shown in Figure 2c, the aromatic carbons in PFP-MSN are observed through  $J$  couplings with the directly bound fluorines. The observed  $^{13}\text{C}$  shifts are consistent with those expected for carbons C5–C9. Surprisingly, each  $^{13}\text{C}$  resonance is involved in double cross-peaks along the  $^{19}\text{F}$  dimension, labeled in red and blue in Figure 2c, representing fluorine sites with similar but discernible chemical shifts. This suggests the presence of two PFP functionalities, which reside on the silica surface in separate average environments and do not change on the time scale of  $(\Delta\nu)^{-1} \cong 1$  ms (where  $\Delta\nu$  is the difference between the corresponding  $^{19}\text{F}$  resonance frequencies in both species). For reasons to be explained later, we denote the molecules represented by “blue” and “red” resonances as PFP-u and PFP-p.

The presence of two nonexchanging conformations of PFP is further verified by the 2D  $^{19}\text{F}$ – $^{19}\text{F}$  DQMAS measurement (Figure 3), which under the excitation and refocusing conditions used here (see figure caption) found only intramolecular



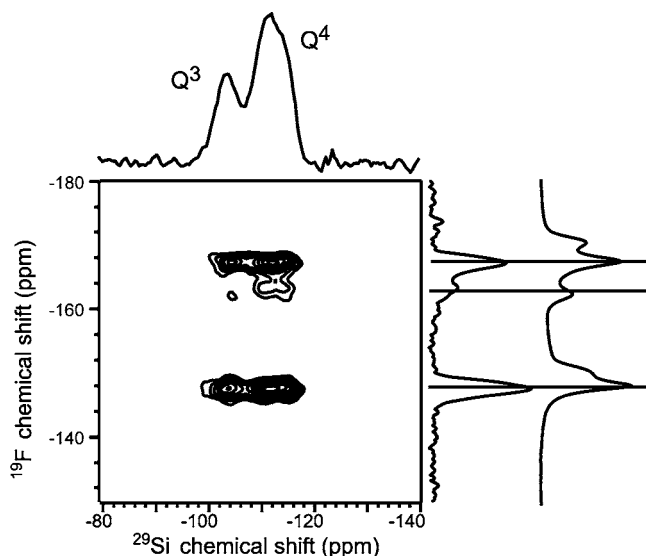


**Figure 4.** 2D  $^{19}\text{F}$ – $^{29}\text{Si}$  CP-based CPMG-HETCOR spectrum of PFP-MSN obtained using  $\nu_{\text{R}} = 40$  kHz,  $\nu_{\text{RF}}^{\text{S}} = 110$  kHz during short pulses,  $\nu_{\text{RF}}^{\text{R}} = 60$  kHz during tangent CP,  $\nu_{\text{RF}}^{\text{S}} = 100$  kHz during short pulses and CP,  $\tau_{\text{CP}} = 20$  ms,  $N_{\text{CPMG}} = 250$  and  $\tau_{\text{CPMG}} = 4$  ms. The data were acquired in 40 rows, with  $\Delta t_1 = 25$   $\mu\text{s}$ , 2000 scans per row,  $\tau_{\text{RD}} = 0.8$  s, and  $\text{AT} = 47$  h. Also shown is the corresponding 1D  $^{19}\text{F}$  MAS spectrum.

correlations between  $^{19}\text{F}$  nuclei, via the dipole–dipole coupling. In the DQ dimension, the signals representing two coupled nuclei resonating at  $\omega_1$  and  $\omega_2$  occur at the sum frequency  $\omega_1 + \omega_2$ , whereas the signals from non-interacting nuclei are suppressed by the DQ filtering.<sup>30</sup> Thus, the spatial proximities between  $^{19}\text{F}$  nuclei can be identified by following the cross-peaks along the horizontal and vertical pathways, as shown in Figure 3 for PFP-p (solid lines) and PFP-u (dashed lines). In the PFP-p functional groups, correlations between all intramolecular neighbors are observed, including the diagonal cross-peaks F5–F9 and F6–F8, and the off-diagonal superpositions of (F5–F6) + (F8–F9) and (F7–F6) + (F7–F8). Similar spectral features are observed for PFP-u, except for the diagonal peaks F5–F9 and F6–F8, which barely exceed the noise level. The differences between relative intensities in  $^{19}\text{F}$  projections in Figures 2c and 3 are insignificant because they result from different spin dynamics involved in  $^{13}\text{C}$ – $^{19}\text{F}$  HETCOR and  $^{19}\text{F}$ – $^{19}\text{F}$  DQ MAS experiments.

To delineate the nature of PFP-p and PFP-u species, we probed their interaction with the silica surface, by measuring a 2D  $^{19}\text{F}$ – $^{29}\text{Si}$  HETCOR spectrum of PFP-MSN (Figure 4). The measurement was enabled by using the CPMG refocusing of  $^{29}\text{Si}$  magnetization,<sup>22</sup> which afforded a 6-fold sensitivity gain (note that without the CPMG refocusing this spectrum would require two months of acquisition time). Notwithstanding the fact that both PFP-p and PFP-u were present in the sample, as evidenced by the  $^{19}\text{F}$  MAS spectrum shown along the  $\omega_1$  dimension, the only observed  $^{19}\text{F}$ – $^{29}\text{Si}$  correlations are associated with the PFP-p species. This demonstrates that the difference between PFP-p and PFP-u functional groups is in their interaction with the surface to which both are covalently bound. All  $^{19}\text{F}$  nuclei in PFP-p groups correlate with Q<sup>3</sup> and Q<sup>4</sup> silicon sites, which indicates that they reside in prone positions with respect to the silica surface and are less mobile. The lack

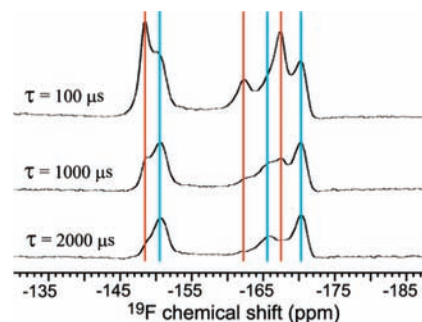


**Figure 5.**  $^{19}\text{F}$  spectra of dried PFP-MSN obtained under MAS at 40 kHz using the spin–echo sequence with  $\tau = 0.1$ , 1.0, and 2.0 ms.

of  $^{19}\text{F}$ – $^{29}\text{Si}$  polarization transfer from the PFP-u species suggests that their aromatic rings are not located near the surface. The increased mobility of the PFP-u species may further contribute to weakening of the  $^{19}\text{F}$ – $^{29}\text{Si}$  dipole–dipole interactions (see the discussion of relaxation data and static NMR spectrum, below). No correlations involving the T sites and the aromatic ring were detected.

The  $^{13}\text{C}$ – $^{19}\text{F}$  HETCOR spectrum of Figure 2c shows that the interaction with the surface shifts the  $^{19}\text{F}$  resonances in PFP-p by 2 to 3 ppm in the direction of higher frequency (deshielded) with respect to PFP-u molecules, but has a very small effect ( $<0.1$  ppm) on the  $^{13}\text{C}$  chemical shifts. An earlier study showed that adsorption of fluoroaromatic molecules (hexafluorobenzene,  $\text{C}_6\text{F}_6$ ) on the surface of alumina has a deshielding effect on the  $^{19}\text{F}$  nuclei compared to the same molecules in the gas phase.<sup>32</sup>

Further corroboration of these assignments was obtained by measuring the transverse relaxation time ( $T_2'$ ) of  $^{19}\text{F}$  nuclei under the spin–echo sequence  $\pi/2$ – $\tau$ – $\pi$ – $\tau$ –detect. The  $T_2'$  values obtained under fast MAS for PFP-u exceeded those for PFP-p by a factor of  $\sim 8$  (12 ms versus 1.5 ms). Indeed, the spectra in Figure 5 show that nuclei in PFP-u and PFP-p were refocused with  $\tau = 0.1$  ms, but only those in PFP-u were observed with  $\tau = 2$  ms, which is consistent with the increased mobility. The existence of two populations of PFP species with different mobilities can be also inferred from the analysis of static  $^{19}\text{F}$  NMR spectrum (not shown) consisting of two superimposed components with the linewidths of  $16 \pm 2$  kHz and  $6 \pm 1$  kHz, which are mainly due to homonuclear  $^{19}\text{F}$ – $^{19}\text{F}$  dipolar interactions. This is a crude approximation, as each component is a superposition of 3 resonances representing F5,9, F6,8 and F7. Still, these values are close, respectively, to those expected for perfluorinated rings that are rigid (PFP-p) and undergo limited motion, such as librational rotation (PFP-u). Note, however, that such mobility alone should not prevent the PFP-u species from being observed in the 2D  $^{19}\text{F}$ – $^{29}\text{Si}$  HETCOR spectrum.

In short, solid-state NMR spectroscopy provided ample evidence for the existence of two distinct populations of PFP functional groups in the MSNs, both of which are covalently bound to the surface, have the same bond structure, but reside in positions described as “prone” (PFP-p) and “upright” (PFP-u) inside the mesopores. The NMR data provide several additional insights about the physicochemical nature of these species. The existence of separate sets of  $^{19}\text{F}$  peaks representing both species shows that they do not change their conformations on the NMR time scale of  $\sim 1$  ms. Based on the  $^{19}\text{F}$ – $^{29}\text{Si}$  CP efficiency, we can estimate that the PFP-p groups are located

(30) Brown, S. P.; Spiess, H. W. *Chem. Rev.* **2001**, *101*, 4125–4155.

(31) Feike, M.; Demco, D. E.; Graf, R.; Gottwald, J.; Hafner, S.; Spiess, H. W. *J. Magn. Reson. A* **1996**, *122*, 214–221.

(32) Budarin, V. L.; Clark, J. H.; Hale, S. E.; Tavener, S. J.; Mueller, K. T.; Washon, N. M. *Langmuir* **2007**, *23*, 5412–5418.

within  $\sim 0.45$  nm from the nearest  $Q^3$  and  $Q^4$  silicon sites. This is a rough approximation, based on the maximum CP intensity being observed at  $\tau_{CP} = 20$  ms and the assumption that the CP dynamics for a rigid pair of spins reaches maximum at  $\tau_{CP,opt} = 1.7/D$ , where the dipolar coupling  $D$  depends on the internuclear distance.<sup>33</sup>

**Theoretical Modeling.** To propose a model of the geometry of the PFP-p species inside the MSNs, we support the solid-state NMR results with theoretical calculations. We point out that the surface of mesoporous silica comprises a complex network of Q and T sites with widely distributed ranges of  $^{29}\text{Si}$  chemical shifts, which reflect their diverse local environments. Our aim is to put forth a simplified model that incorporates the basic chemical properties of the PFP-MSN surface and is consistent with both experimental and theoretical studies. Earlier *ab initio* studies of the interaction between an isolated pair of water and  $\text{C}_6\text{F}_6$  molecules have shown that  $\text{C}_6\text{F}_6$  can act as a lone-pair acceptor and interact with the oxygen center of  $\text{H}_2\text{O}$  forming a dimer with a binding energy of about  $-8$  kJ/mol.<sup>34</sup> Due to the electron-withdrawing effect of the fluorine atoms and the resulting electron deficiency of the  $\text{C}_6\text{F}_6$  aromatic  $\pi$ -system, the oxygen of water is located approximately 0.32 nm from the center of the molecule, with both hydrogen atoms pointing away from the ring. This is in contrast to water–benzene interaction, which leads to a different  $\pi$ -electron distribution and results in formation of a weak hydrogen bond with water, such that both hydrogen atoms point toward the ring.<sup>34</sup> Following the Lewis acid and base concept, in the  $\text{C}_6\text{F}_6$ – $\text{H}_2\text{O}$  system the oxygen atom acts as a Lewis base and the aromatic ring may exhibit Lewis acidity, whereas in the  $\text{C}_6\text{H}_6$ – $\text{H}_2\text{O}$  system water plays the role of an acid. These properties of the PFP functional groups are relevant to surface science and catalysis, as will be pointed out in the Conclusion.

The above-mentioned *ab initio* studies of the  $\text{C}_6\text{F}_6$ – $\text{H}_2\text{O}$  system<sup>34</sup> evoke a possibility that pentafluorophenyl groups of the PFP functionalities act in a similar fashion as a lone-pair acceptor and interact with the oxygen atom of the MSN surface. We have optimized the geometries of  $\text{C}_6\text{F}_6$  interacting with two major oxygen species on the MSN surface: the oxygen atoms of silanol groups,  $\text{HO-Si}(-\text{OSi}\equiv)_3$ , and siloxane bridges,  $(\equiv\text{SiO}-)_3\text{Si-O-Si}(-\text{OSi}\equiv)_3$ . The surface models for these species were created based on  $\beta$ -cristobalite structure ( $\text{Si-O}$  bond length = 0.161 nm and  $\text{Si-O-Si}$  bond angle =  $146.4^\circ$ ),<sup>35,36</sup> because the local structure of MSN is similar to that of amorphous silica<sup>37,38</sup> and X-ray work on amorphous silicas suggests that their structure most closely resembles that of  $\beta$ -cristobalite.<sup>39</sup> The  $\text{Si-O-H}$  bond angle was initially set to  $121^\circ$ .<sup>40</sup> The silicon atoms that do not carry the full complement of hydroxyl or siloxane bridges were terminated by hydrogen

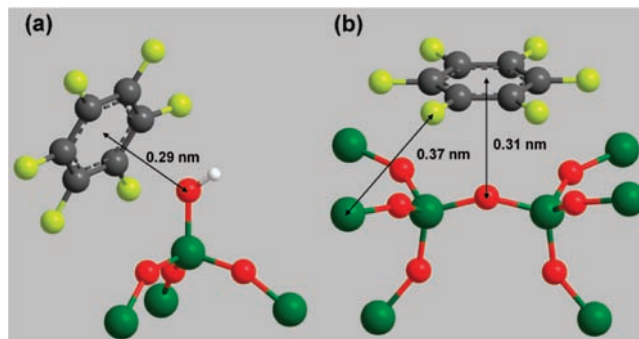


**Figure 6.** The optimized geometries of (a)  $\text{C}_6\text{F}_6$ –silanol and (b)  $\text{C}_6\text{F}_6$ –siloxane models. Silicon atoms are green, oxygen atoms are red, carbon atoms are gray, fluorine atoms are yellow, and hydrogen atom is white. Silanol hydrogen is the only one shown.

atoms. The structure of the Si-containing clusters was fixed during the optimization, except for the OH moieties of the silanol groups. The resulting geometries of the  $\text{C}_6\text{F}_6$ –silanol and  $\text{C}_6\text{F}_6$ –siloxane environments are shown in Figure 6. In both structures, the center of the  $\text{C}_6\text{F}_6$  molecule appears to be located near the oxygen atom.

In the optimized  $\text{C}_6\text{F}_6$ –silanol geometry (Figure 6a), the distance between the oxygen atom and the center of mass of the aromatic ring and the interaction energy are calculated to be  $d = 0.29$  nm and  $\Delta E = -5.6$  kJ/mol, respectively. Furthermore, five fluorine atoms of the  $\text{C}_6\text{F}_6$  are separated from the nearest silicon atom ( $Q^3$  site) by more than the NMR estimate (0.45 nm). The hydrogen bonds between the surface silanols and the fluorine atoms do not seem to form on the silica surface, which is consistent with the previous studies of the  $\text{C}_6\text{F}_6$ – $\text{H}_2\text{O}$  system.<sup>34</sup> This result is not surprising, because fluorine that bonds to  $\text{sp}^2$  carbon is a poor hydrogen-bond acceptor.<sup>40,41</sup> The geometry shown in Figure 6a suggests that on the “real” MSN surface the  $\text{C}_6\text{F}_6$ –silanol interaction can be affected by steric hindrance within the system. Furthermore, fast librational motions of the silanol OH moieties<sup>40</sup> make it difficult for the aromatic ring and the silanol oxygen to interact with each other.

An optimized geometry of the  $\text{C}_6\text{F}_6$ –siloxane system is shown in Figure 6b. In this case, the  $\text{C}_6\text{F}_6$  molecule lies flat above the siloxane oxygen at a distance of  $d = 0.31$  nm with all fluorine atoms having one or more neighboring silicon atoms within 0.45 nm. The computed interaction energy ( $\Delta E = -11.0$  kJ/mol) is larger than that for the  $\text{C}_6\text{F}_6$ –silanol model. The mobility of the  $\text{C}_6\text{F}_6$  molecule under such conditions is expected to be limited.

The  $\text{C}_6\text{F}_6$ –siloxane system is further studied by theoretical calculation of the  $^{19}\text{F}$  chemical shift. The computation of the  $^{19}\text{F}$  chemical shift of an isolated  $\text{C}_6\text{F}_6$  molecule yielded  $-165.2$  ppm, which is close to the reported value in the gas phase ( $-167.75$  ppm).<sup>32</sup> The  $^{19}\text{F}$  chemical shift of the  $\text{C}_6\text{F}_6$  molecule in the optimized  $\text{C}_6\text{F}_6$ –siloxane system was calculated to be  $-155.9$  ppm (average of all six fluorine atoms), which demonstrates that the interaction of  $\text{C}_6\text{F}_6$  molecules with the siloxane oxygen has a deshielding effect on the  $^{19}\text{F}$  nuclei compared to the  $\text{C}_6\text{F}_6$  in the gas phase. This deshielding effect is in agreement with  $^{19}\text{F}$  NMR data, although its size exceeds the experimental value of  $\sim 3$  ppm. However, on the “real” surface, the aromatic ring of the PFP-p species is not located in the geometry where it maximally interacts with the siloxane oxygen because of the constraints imposed by the propyl chain, as well as the physical topology and chemical structure (e.g., concentration of silanol

(33) Amoureux, J. P.; Pruski, M. *Mol. Phys.* **2002**, *100*, 1595–1613.

(34) Danten, Y.; Tassaing, T.; Besnard, M. *J. Phys. Chem. A* **1999**, *103*, 3530–3534.

(35) Shimura, T.; Misaki, H.; Umeno, M.; Takahashi, I.; Harada, J. *J. Cryst. Growth* **1996**, *166*, 786–791.

(36) Peacor, D. R. *Z. Kristallogr.* **1973**, *138*, 274–298.

(37) Beck, J. S.; Vartuli, J. C.; Roth, W. J.; Leonowicz, M. E.; Kresge, C. T.; Schmitt, K. D.; Chu, C. T. W.; Olson, D. H.; Sheppard, E. W.; McCullen, S. B.; Higgins, J. B.; Schlenker, J. L. *J. Am. Chem. Soc.* **1992**, *114*, 10834–10843.

(38) Edler, K. J.; Reynolds, P. A.; White, J. W. *J. Phys. Chem. B* **1998**, *102*, 3676–3683.

(39) Frondel, C. *Am. Mineral.* **1979**, *64*, 799–804.

(40) Kobayashi, T.; DiVerdi, J. A.; Maciel, G. E. *J. Phys. Chem. C* **2008**, *112*, 4315–4326.

(41) Howard, J. A. K.; Hoy, V. J.; O'Hagan, D.; Smith, G. T. *Tetrahedron* **1996**, *52*, 12613–12622.

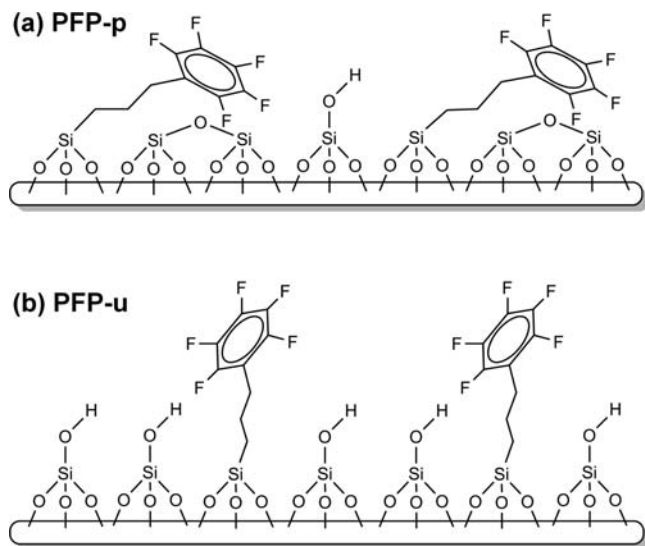


**Figure 7.** The schematic representation of (a) PFP-p and (b) PFP-u functional groups on the silica surface. The aromatic rings of PFP-p interact with the siloxane oxygen, whereas those in PFP-u are located further from the surface and are more mobile.

groups) of the MSN surface. Besides, even the PFP-u species are not truly isolated in the narrow pore of the MSN materials. Thus, the difference in  $^{19}\text{F}$  chemical shifts between PFP-p and PFP-u is likely to be smaller than that calculated for the  $\text{C}_6\text{F}_6$ -siloxane model.

The theoretical calculations suggest that a feasible model representing the PFP-p species is one in which the aromatic ring of the PFP group is located above the siloxane oxygen in parallel to the MSN surface (Figure 7a). This geometry is consistent with the following NMR results: (1) the  $^{19}\text{F}$  nuclei in PFP-p groups are located within  $\sim 0.45$  nm from the nearest  $\text{Q}^3$  and  $\text{Q}^4$  silicon sites, (2) the mobility of the ring is restricted compared to PFP-u, (3) the  $^{19}\text{F}$  nuclei of the PFP-p are deshielded by the interaction with silica. Due to the above-mentioned steric constraints, only a fraction of the PFP groups can be located above the siloxane oxygen as PFP-p, whereas the others are confined to PFP-u positions. The most likely structure of PFP-u is shown in Figure 7b. We should emphasize that the designation of PFP-u molecules as “upright” does not imply that they assume rigid vertical positions on the surface. The NMR data showed reduced  $^{19}\text{F}$  line width and slower transverse relaxation in PFP-u, most likely as a result of librational flips or rotations. Whereas this mobility may slow

down the  $^{19}\text{F}$ - $^{29}\text{Si}$  CP process, the absence of resonances representing PFP-u in the  $^{19}\text{F}$ - $^{29}\text{Si}$  HETCOR spectrum and the change in  $^{19}\text{F}$  chemical shifts demonstrate that these species are more distant from the MSN surface than PFP-p.

## Conclusion

The NMR results and the theoretical calculations presented in this study showed that the PFP-MSN material hosts two types of covalently bound PFP species with similar bond topologies but different conformations: the PFP-p groups with the aromatic rings located above the surface siloxanes and the PFP-u molecules in the roughly upright position. The fundamental understanding of the silica surface provided by this investigation can be used to enhance the catalytic performance in a predictable way. The interaction energy calculated for the  $\text{C}_6\text{F}_6$ -siloxane model system is larger than the adsorption energy of water molecules to dehydrated surface of a mesoporous silica material at low vapor pressure.<sup>42</sup> Since surface siloxanes of MSN materials are easily hydrolyzed to form silanols by water adsorption even at room temperature,<sup>43,44</sup> enhancing the hydrophobic character of these materials by protecting the siloxanes from water should be beneficial for their catalytic applications.

Indeed, in a forthcoming publication we will report on the design of a bifunctional MSN-based catalyst containing an acidic catalytic site and PFP functionalities for an esterification reaction. The presence of PFP improved considerably the catalytic performance, which is attributed to efficient expulsion of the byproduct (water) from the PFP-coated mesochannels. Further experimental and theoretical investigations are underway to describe the behavior of the PFP functional groups on the MSN surfaces in the presence of solvents.

**Acknowledgment.** This research was supported at the Ames Laboratory by the U.S. Department of Energy, Office of Basic Energy Sciences, under Contract No. DE-AC02-07CH11358. We would also like to thank the U.S. Department of Energy, Office of Energy Efficiency and Renewable Energy (Grant No. DE-FG26-0NT08854), for financial support.

JA105007B

(42) Cauvel, A.; Brunel, D.; DiRenzo, F.; Garrone, E.; Fubini, B. *Langmuir* **1997**, *13*, 2773–2778.

(43) Matsumoto, A.; Sasaki, T.; Nishimiya, N.; Tsutsumi, K. *Langmuir* **2001**, *17*, 47–51.

(44) Matsumoto, A.; Tsutsumi, K.; Schumacher, K.; Unger, K. K. *Langmuir* **2002**, *18*, 4014–4019.